

# Evolvable Skin Electronics by In Situ and In Operando Adaptation

Kyun Kyu Kim, Joonhwa Choi, Joon-Hong Kim, Sangwook Nam, and Seung Hwan Ko\*

Latest developments in thin-film electronics have put skin electronics in the limelight. Integration of multiple skin sensors and wireless power transferring ability are cardinal components for continuous acquisition of the human signals, enabling higher level of applications in wearable healthcare and AR/VR devices. Skin sensor is considerably influenced by target body parts and users where it is attached, and thus face various design adjustments for the best performance. However, most skin electronics using conventional fabrication methods have a fixed design for specific targets and users only and face great challenge when they need design changes, for it has to re-initialize entire fabrication process even for the simplest design modification. Here, in situ and in operando adaptation (SOA) is presented, a revolutionary customizable electronic fabrication platform that allows simultaneous evolvable design modification and addition of new functionality to original skin electronics while they are in operation on a human skin. SOA renders immediate response to various user specifications possible, offering concurrent customization for various wearable and wireless applications including human physiology/motion sensors. Furthermore, SOA offers simultaneous impedance optimization in different body parts and users which enables on-skin wireless power supply. These findings will prove a boon to the development of customizable wearable skin-like electronics.

logical advances, devices now integrate multiple components that allow multi-functional measurement capabilities.<sup>[6,9,10]</sup> Moreover, radio frequency (RF) energy harvesting module is widely used as an effective and practical layout for untethered and battery-less power supply.<sup>[10,14–16]</sup> These technologies are cardinal components for continuous measurement of multiple signals generated from the body,<sup>[10,12]</sup> rendering a wide range of fields in wearable healthcare and augmented and virtual reality (AR and VR) devices<sup>[14]</sup> possible.

Most previous researches, however, focused on enhancing the performance of the device itself and lacks consideration for the various characteristics difference of the individual who wears the sensors. Such tendency restricts the device from carrying out diverse tasks and adjusting to different environments during its practical utilization. For instance, active adaptation to various user specifications which entails different corresponding combination and arrangement of the sensing elements is required. Moreover, adequate response to

unforeseen variables, such as human body radio interference, are essential in terms of costs and efficient production of the device. Electromagnetic interference variance entailed by each individual and different body parts require specific designs of power transmission antenna.<sup>[17–21]</sup>

To address these needs, design adjustments are inevitable during the management of such variables; however, the conventional fabrication methods showed limitation in adapting

## 1. Introduction

Latest developments in wearable electronics have sparked an interesting innovation in electronic skin,<sup>[1–3]</sup> which provides a skin-compliant direct human-machine interface. These devices are composed of conductors that exhibit high mechanical compliance; thin-film electrodes,<sup>[4–6]</sup> serpentine mesh layouts,<sup>[7–10]</sup> and patterns of stretchable materials.<sup>[11–13]</sup> Thanks to techno-

K. K. Kim  
Soft Robotics Research Center  
Seoul National University  
Seoul 151-744, Republic of Korea

K. K. Kim, J. Choi, S. H. Ko  
Applied Nano and Thermal Science Lab  
Department of Mechanical Engineering  
Seoul National University  
1 Gwanak-ro, Gwanak-gu, Seoul 151-742, Republic of Korea  
E-mail: maxko@snu.ac.kr

J.-H. Kim, S. Nam  
Institute of New Media Communication  
School of Electrical and Computer Engineering  
Seoul National University  
Seoul 151-742, Republic of Korea

S. H. Ko  
Institute of Advanced Machines and Design  
Seoul National University  
Seoul 08826, Republic of Korea  
S. H. Ko  
Institute of Engineering Research  
Seoul National University  
Seoul 08826, Republic of Korea

 The ORCID identification number(s) for the author(s) of this article can be found under <https://doi.org/10.1002/adfm.202106329>.

DOI: 10.1002/adfm.202106329

to changes by relying on additive processes (inkjet,<sup>[22–24]</sup> deposition,<sup>[8,12]</sup> and replication of master mold<sup>[13]</sup>) or cutting processes,<sup>[7,25,26]</sup> where it is difficult to change original design. Hence, the asynchronization of design adjustments and fabrication in conventional methods involved a full re-initialization (mask redesign or restart of fabrication process) of the entire process even for the simplest design modification.

In order to expedite advancement in these processes, we have developed a design-fabrication synchronized ultrathin electronic development platform for active electronic customization: In situ and in operando adaptation (SOA). This laser-based rewritable process involves sintering and ablation of metal nanoparticles, allowing the previous printed circuit to be erased or drawn for alternation or extension to add new functionality or to tune the device performance. SOA offers a flexible sensor customization ability allowing the original design to generate various derivatives for different purposes without discarding their original products. The original device can be customized according to different user specifications such as measuring skin conditions and human physiological signals. A

precise and rapid vertical interconnect access (VIA) depth control allows more than two separate wires to be crossed in different thin layers under 3  $\mu\text{m}$ . Moreover, the entire process is driven under rapid mask-less bottom-up process which involves drawing/erasing speed of 20  $\text{mm}^2 \text{s}^{-1}$ . SOA provides an efficient customization framework which enables concurrent optimization of the system's impedance. Since there is considerable impedance mismatch when applying identical products to other body parts and different users, the antenna design is simultaneously adjusted to accommodate the resonance impedance of each state. Furthermore, the system further achieved wireless charging and battery-less operation capability above human body.

### 1.1. In Situ and In Operando Adaptation

The systematic overview of SOA is shown in Figure 1a. Device attachment locations of the skin-like electronics vary with the various applications that they hold. Conventional studies in

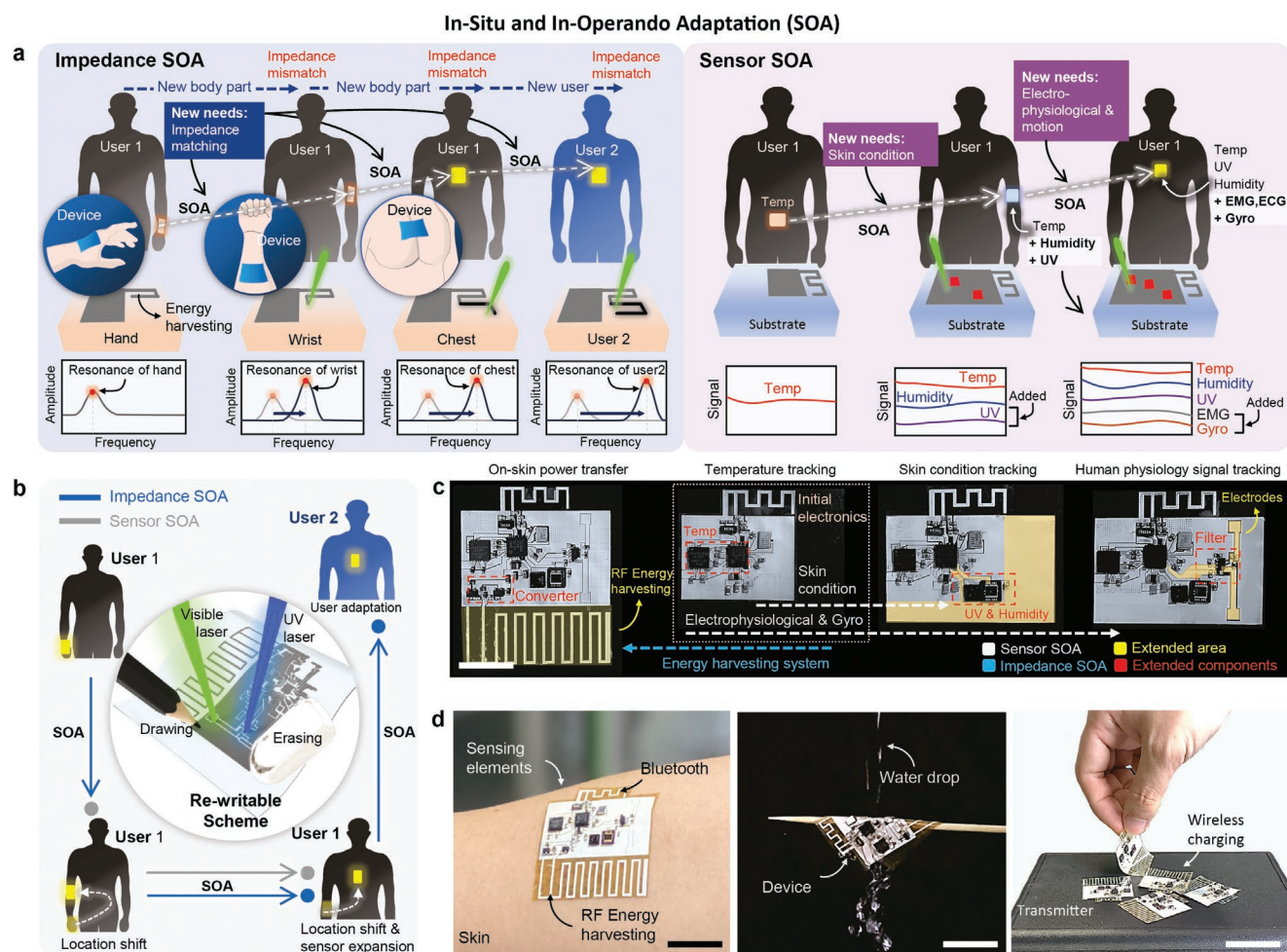


**Figure 1.** In situ and in operando adaptation (SOA). a) Schematic illustration of the impedance and sensor SOA. Active impedance adaption of different body location and users is available through impedance SOA. b) The device is actively adapted to the various user demands and corresponding attachment locations through impedance and sensor SOA. SOA is based on the laser rewriting of metal nanoparticles. c) Developed device according to user specifications and body impedance through SOA. Scale bar: 10 mm. d) Images of the developed skin electronic device including various sensing elements with on-skin power transferring ability. Scale bars: 15, 15, and 20 mm, respectively.

untethered/battery-less devices apply identical designs of energy harvesting antenna regardless of its attaching location of our body.<sup>[12,16]</sup> However, substantial power attenuation is expected due to impedance mismatch on different body parts.<sup>[18,21,27,28]</sup> Mismatch also occurs between users given their unique tissue and bone arrangements.<sup>[29,30]</sup> Conventionally, an intensive simulation is required to optimize the antenna structure.<sup>[17,18,20]</sup> In contrast, SOA allows continuous real-time scanning of various designs to obtain the optimal antenna structure, which can be actively optimized according to the body part (e.g., hand, wrist, chest) and user characteristics.

SOA provides a concurrent adaptation to user specifications in a single device. As shown in sensor SOA, the device actively expands its design to accommodate increasing user demands, from temperature measurements to acquisition of skin condition, human physiological signals, and motions signals. The desired sensors, such as humidity, ultraviolet (UV), electromyography (EMG), and gyroscopic sensors, are added to comply with user needs, unlike conventional methods, in which modifications are not possible.

Figure 1b shows that the device immediately responds to changes in unforeseen new user specifications and the impedance of the corresponding location through SOA. SOA is based on a rewriting scheme with two main features: (1) additive manufacturing by visible wavelength laser sintering of metal nanoparticles and (2) subtractive manufacturing through ultraviolet laser ablation. Each laser source selectively converts silver nanoparticles into electrically connected layers or removes existing electrical patterns (Video S5, Supporting Information).

This process allows electrical connections to be continuously drawn and erased above the ultrathin substrate (colorless polyimide; CPI) without requiring any preparation process (e.g., photomasking, molding). The bottom-up stacking of multiple layers enables the rapid and efficient development of devices with diverse functionality. The details of fabrication are available in section Methods.

Figure 1c shows devices developed using the proposed SOA (Figure S1, Supporting Information). The basic electronics contains a microcontroller unit (MCU) connected to a temperature sensor. Sensor SOA offers flexible customization for different applications by extending the area and creating electrical paths. An optimized radiofrequency (RF) energy harvesting system placed on the human skin can also be developed through impedance SOA. The photograph in Figure 1d shows a device attached to the wrist to provide physiological measurement components with on-skin wireless power transmission. The device can be fully folded by water drops, and several devices can be simultaneously charged through wireless power transmission. The exploded schematic of the device and connected elements are depicted in Figures S2 and S3 (Supporting Information), respectively.

## 1.2. Real-Time In Situ Design Customization of Skin Electronics by SOA

Figure 2 illustrates the core fabrication process of SOA. The CPI is uniformly coated and annealed on a glass substrate, and the thickness of the CPI film is determined to be 3  $\mu\text{m}$

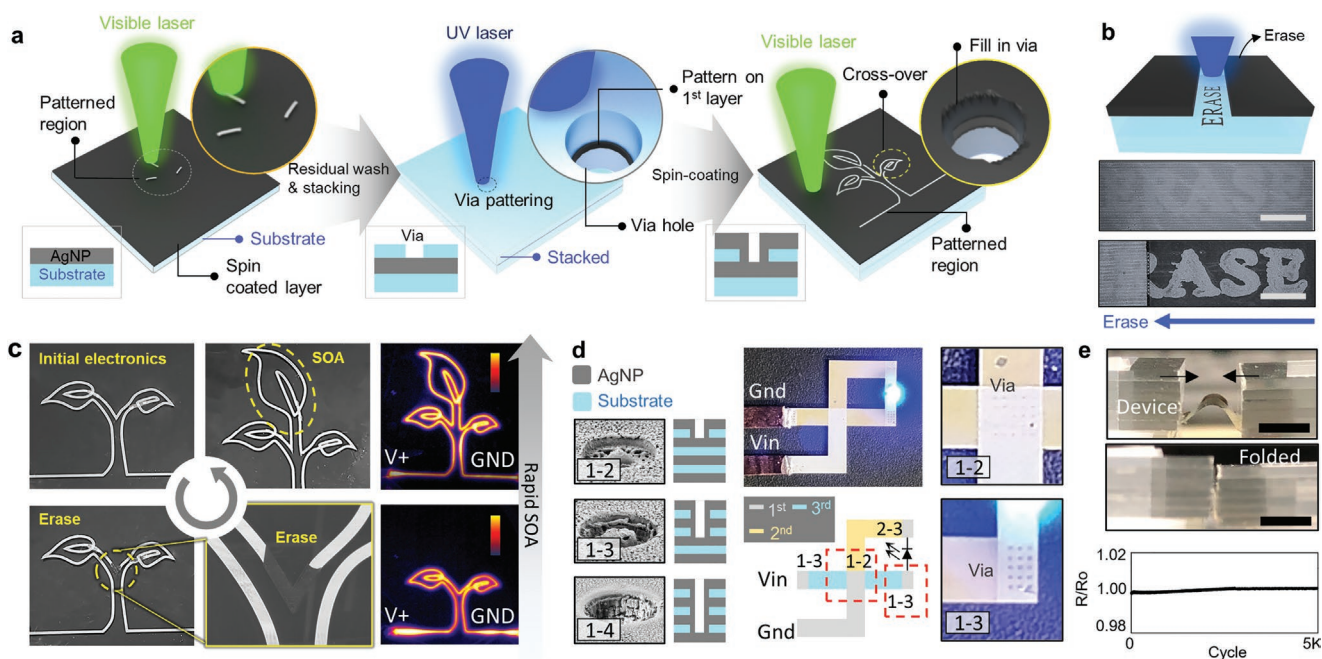


**Figure 2.** Real-time in situ design customization of skin electronics in SOA. a) Schematic illustration of drawing of first layer: stacking and VIA formation and drawing of second layer. b) Illustration of erasing the top layer electrode with accompanying optical images. Scale bars, 200  $\mu\text{m}$ . c) Concurrent prototyping of an electronic sprout. Sprout has been grown as shown in the thermographic image. d) SEM images and corresponding illustration of the controlled VIA of four-layer device and the demonstration of the selective VIA control of the three-layer circuit system. e) Dynamic electrical response of the patterned electrode under 5 K of folding cycles. Scale bars: 10 mm

by adjusting the speed of the revolution and the duration time. The fabricated AgNP ink is then spin-coated over the layer. 532 nm wavelength laser is focused at the AgNP layer to selectively convert the AgNPs into a designed metal pattern and they adhere strongly to the substrate<sup>[31,32]</sup> as shown in Figure 2a. The surrounding nonsintered residues are easily cleaned and removed by washing with polar solvents (e.g., ethanol, water). In order to form an insulation sheet, additional CPI solution is then deposited into the pre-fabricated circuit. VIAs are formed by 355 nm UV laser drilling. After simply spin-coating the AgNP onto the post-processed layer, AgNP ink spontaneously filled the drilled VIAs. A subsequent sintering and washing process is followed to create a two-layer electronic device.

During the fabrication, the device undergoes not only the “drawing” but also the “erasing” process as depicted in Figure 2b. The low-power UV laser (26 mW, 0.01 mm s<sup>-1</sup>) selectively ablate the upper AgNPs without damaging the substrate and the previously patterned bottom layer electrode (Figure S14, Supporting Information). The previously patterned letter “ERASE” appears after the erasing process as shown in the figure. Erasing process makes the use of an existing circuit by creating empty space to draw a new circuit or by splitting the electrode into several independent electrical lines.

An example of concurrent design modification through SOA is demonstrated in Figure 2c. An electrical sprout is grown by the initial drawing process in the Eulerian path with crossovers. The center part of the stem is removed by the erasing process prior to further plant growth. New branches would then expand from the middle, forming an enlarged electrical path as verified by a thermographic image.

Precise VIA depth control of highly stacked four-layer electronics is demonstrated as depicted in Figure 2d. Easy manipulation of depth control is possible by varying the laser power; the connections does not go through the entire layers at low UV power. SEM image verifies the controllability of the VIA connections of the inner layers and the numbers indicate where the connections are formed. A three-layer circuit system demonstrates that the depth-controlled VIA is well-formed at the center of the circuit. VIA connects the top and the middle layer without creating a short circuit between the bottom layer; therefore, LED stably lightened up where the red line illustrates the current flow from V<sub>in</sub> to Gnd. The connection at the bottom LED electrode requires a through VIA, and the magnified optical image depicts the difference of the VIAs at the center and the electrode at the right-side. As shown in Figure S4 (Supporting Information), VIAs were formed with 20 μm size of diameter, where the optimum number of VIA density was found at #20/mm<sup>2</sup>. Excessive amount of VIAs reduces the effective conducting area and eventually increases the resistance between the electrodes. An example of the through VIA and uniform step coverage can be observed in the scanning electron microscope (SEM) image. EM provides a powerful solution for electronics development for rapid evaluation and re-designing. A dynamic cycle response under complete folding is depicted in Figure 2e, where it demonstrates the electrical stability with the aid of its thin characteristics.

### 1.3. In Operando, Real-Time Impedance Optimization of Skin Electronics by SOA

SOA proposes a novel method for optimizing the impedance of the system as illustrated in Figure 3a. SOA discovers the design of the matching component for an unknown impedance system in a real-time manner. The system consists of a series of RLC (resistor, inductor, and capacitor) components, where the capacitance varies as the upper-layer area increases during SOA. A thermochromic pigment coated above the resistor (heater) serves as a power indicator. In the phasor diagram, the phase varies during SOA, and the optimum point is identified when the imaginary reactance is offset by the increased capacitance (Video S1, Supporting Information).

As a proof of concept, we prepared four impedance systems connected to LEDs (light-emitting diodes) and with the initial root antenna drawn as shown in Figure 3b. SOA expands or shortens the antenna following the meandering monopole design. Each LED is activated at the different points along the antenna structure. The brightness of each LED according to the antenna growth is shown in Figure 3c. A system with a high impedance (Z<sub>4</sub>, four inductors connected in series) activates the LED at earlier along the antenna growth and for a longer period than that with a low impedance (Z<sub>1</sub>, single inductor connected) (Video S2, Supporting Information). The real-time activation of the four LEDs is shown in Figure 3d. The opposite response is observed in the four LEDs during SOA erasing.

To validate the proposed optimization process, we construct a theoretical model predicting the real-time activation of the LEDs. The Friis equation relates the receiving power with the transmitted power as  $P_r/P_t = (1 - |\Gamma_r|^2)(1 - |\Gamma_t|^2)(\lambda/4\pi R)^2 G_t G_r$ , where  $\Gamma_r$ ,  $\Gamma_t$ ,  $P_r$ ,  $P_t$ ,  $\lambda$ ,  $R$ ,  $G_r$ , and  $G_t$  denote the reflection coefficients of the receiver and transmitter, received power, input power, wavelength, distance, and gains of the receiver and transmitter, respectively.<sup>[29]</sup> Assuming that the gain-to-power ratio of the transmitter and the distance are constant, the equation reduces to  $P_r = cG_r(1 - |\Gamma_r|^2)$ , where  $c$  denotes a constant. Coefficient  $\Gamma_r$  is defined as  $(Z_a - Z_R^*)/(Z_a + Z_R)$ , where  $Z_a$  is the impedance of the receiving antenna and  $Z_R$  is the reference impedance of the circuit.<sup>[30]</sup>  $P$  and  $Z_a$  are obtained using the finite element method, and the theoretical values are determined to match the experimental values. Thus, the unknown impedance of the first LED is  $Z_R = 15 + 82i \Omega$ .

Figure 3e shows impedance SOA used for different users. The height ( $h$ ) of the RF energy harvesting MIFA is optimized through SOA by continuously scanning the design. When attaching the device from a well-matched design for user 1 ( $h = 10$  mm) to user 2, a considerable difference in the resonance frequency is observed. As shown in Figure 3f, the impedance of the antenna is rapidly matched through impedance SOA to the working frequency by reducing the antenna height ( $h = 75$  mm).

Figure 3g shows active adaptation to different body parts. A severe impedance mismatch from the working frequency is observed when an identical design with  $h = 10$  mm is attached to each body part. Impedance SOA determines the optimal height of each body part (hand:  $h = 75$ ; wrist:  $h = 6.5$ ; chest:  $h = 9.7$ ), allowing each S11 parameter to change perfectly to the working frequency. Figure 3h shows the optimized device on hand. Five LEDs arranged at the corner of a star show the

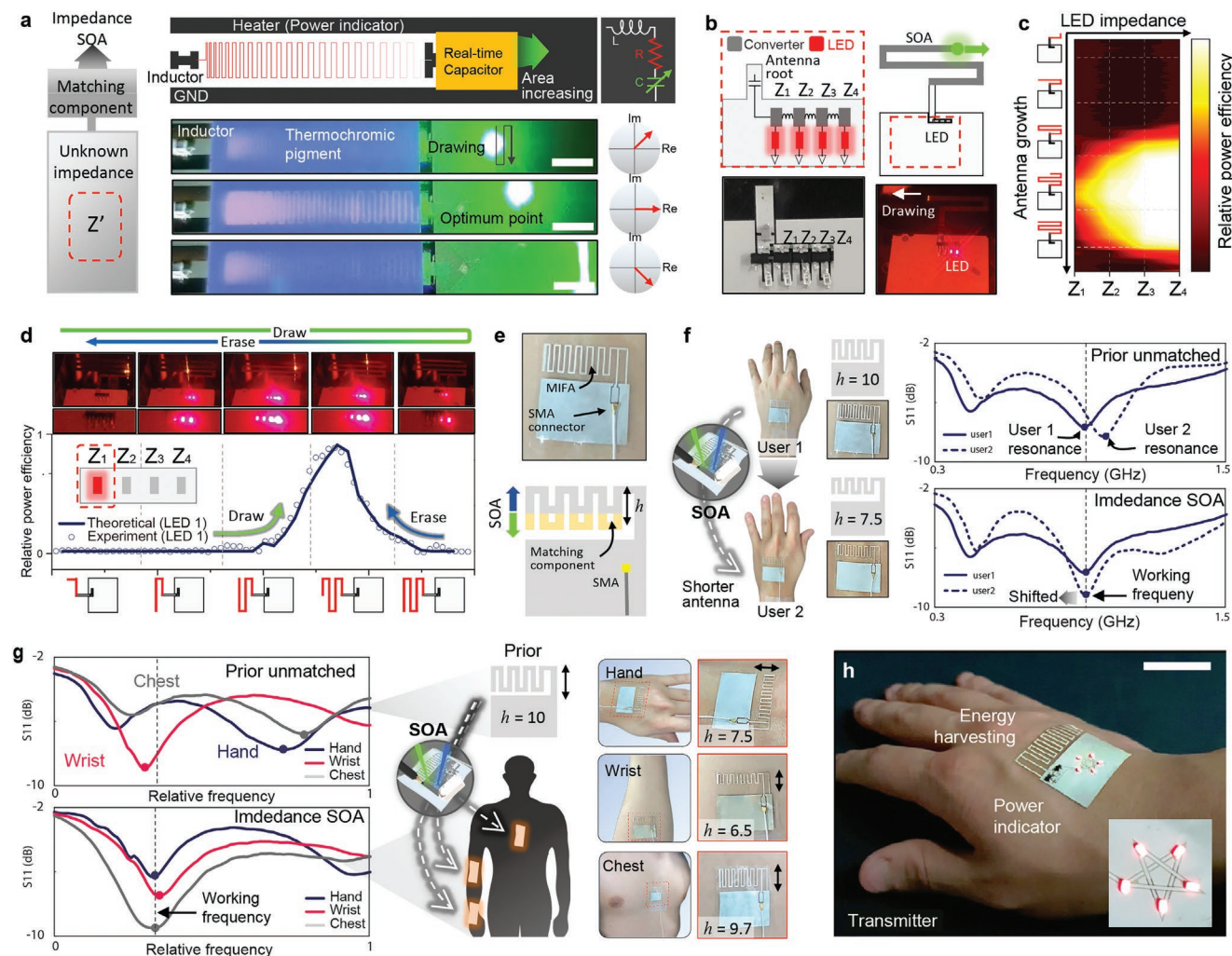


**Figure 3.** In operando, real-time impedance optimization of skin electronics by SOA. a) Schematic illustration of SOA where it optimizes the impedance of an unknown system in a real-time manner. A virtual analogue system connected with unknown inductor is shown. Power fluctuation on heater can be observed during the drawing of the capacitor. Scale bars, 5 mm. Corresponding circuit and the phasor diagram are shown on the right. b) Electrical system with unknown impedance where the capacitor and inductors are connected in series. Each LED indicates of virtual electrical system with different impedances. The matching component (antenna) is simultaneously modified through SOA. c) Relative LED luminance as a function of the antenna growth. d) Captured image of each LED's real-time brightness during the impedance SOA. Real-time luminance distribution of the LED ( $Z_1$ ) and comparison between the theoretical values are shown below. e) User adaptation through SOA which involves antenna height ( $h$ ) modification. The device is connected with SubMiniature version A (SMA) connector for S-parameter measurement. f) The device adapted to the new user (user 1), where the resonance successfully shifts to the working frequency. g) Device adapts to different body locations (Hand, wrist, and chest) through impedance SOA. Resonances of each device well-matched to the targeted working frequency. h) Optimized design above hand with five LEDs lightens up with wireless power transfer. Scale bar: 20 mm

on-skin power receiving capability (Figure S5, Supporting Information). In addition to design modification of antennas, SOA also provides an active adaptation of unexpected radio interference (e.g., high frequency interference) through extension of filtering components (resistor and capacitor) (Figure S6, Supporting Information).

### 1.4. In Operando Addition of New Sensor Functionalities by SOA

An exemplary development scenario involving active customization is illustrated in Figure 4. The main fabrication (Figure 4a) comprising the core functions includes a MCU and

a temperature sensor acquiring measurements at a sampling rate of 50 Hz. The device can be expanded to accommodate new user requirements for measuring the skin condition. For instance, humidity and UV sensors are added through SOA. The extended areas are outlined in yellow, and the boundaries are visible in the optical image. Figure 4b shows the device attached on top of the wrist for monitoring temperature, humidity, and UV radiation according to the wrist tilting.

Figure 4c shows the microscopic process performed during sensor expansion by SOA. For adding a UV sensor, the microscopic image shows the erasing, area expansion, and wiring processes. The schematics for expanded serial communication are also observed. Another sensor SOA for physiological

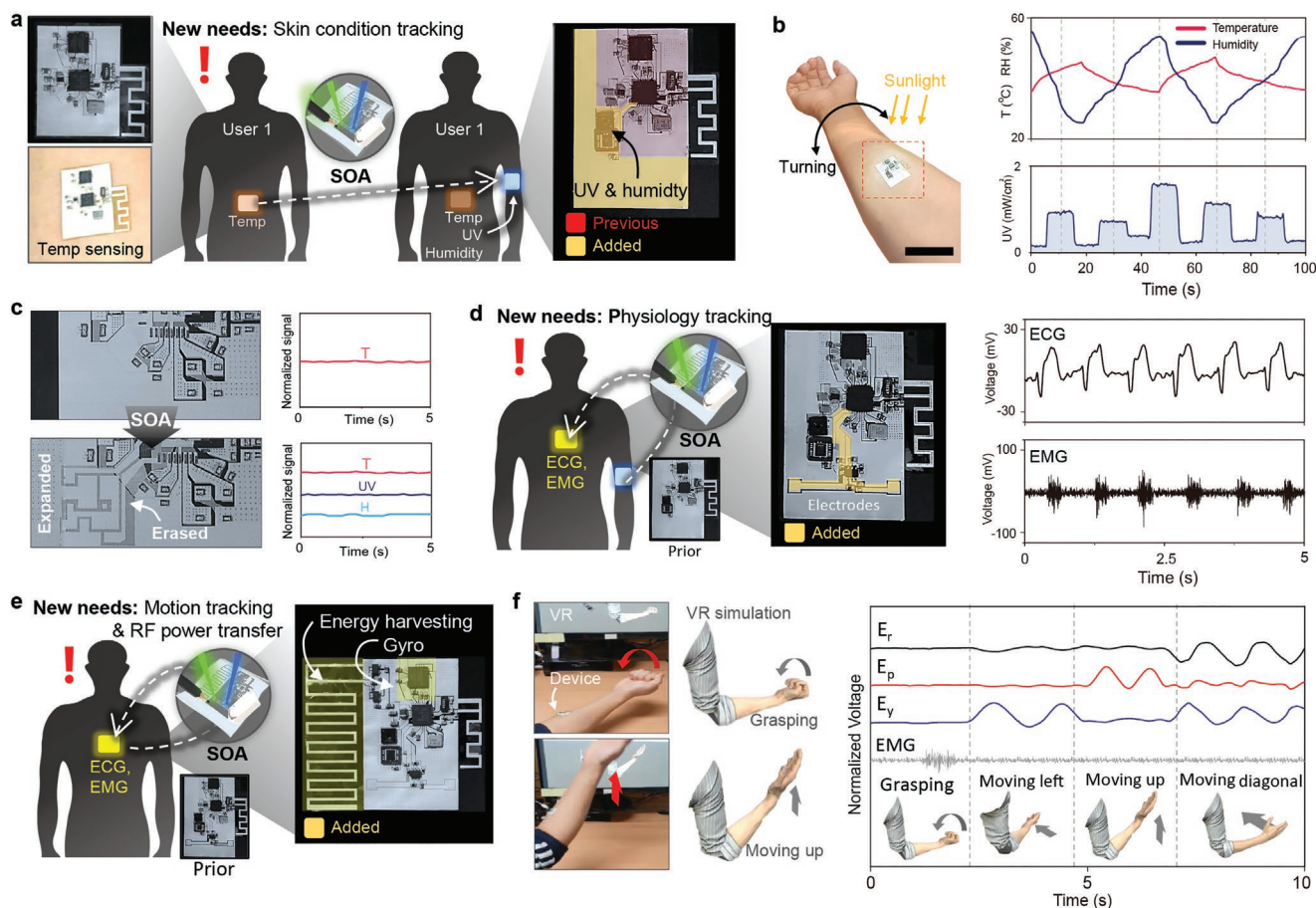


**Figure 4.** In operando addition of new sensor functionalities by SOA. a) Original sensor contains fundamental devices of MCU and temperature sensor. The device actively customized to the new user demands of skin condition tracking by adding UV and humidity sensing elements. The yellow color in the figures represents the expanded regions by SOA. b) Measuring of various factors that relates to skin conditions (real-time temperature, UV, and humidity). Scale bar: 40 mm. c) Corresponding optical images of erase and expansion. Data achieved from the original mother generation and the extended sensor data of UV and humidity signals of the second generation is shown on the right. d) Active adaptation of new user needs for human physiology measurement. New nodes for electrophysiology electrodes are extended and the ECG and EMG signals are successfully measured. e) Sensor and impedance SOA for wireless motion tracking with RF power transfer. Energy harvesting antenna and gyroscopic sensor is added. f) The developed sensor is used to control virtual hand in real-time, and the measured gyroscopic and EMG signals are shown on the right.

tracking is included, as shown in Figure 4d. The nodes for a bandpass filter and skin electrodes are included. This device can be attached above the chest and wrist for measuring electrocardiography and EMG signals (Figure S10, Supporting Information).

Figure 4e shows SOA for human motion tracking and wireless power transmission. A gyroscopic sensor is included for motion measurement, and a meander-line inverted F antenna (MIFA) with AC/DC conversion is added for RF energy harvesting. The device is fully charged in an hour and a half using a 915 MHz transmitter and the optimized antenna design for on-skin applications (Figure S5 and Note S1, Supporting Information). The device is further attached to the wrist to remotely control a virtual hand, as shown in Figure 4f and Video S3 (Supporting Information). Measurements of roll, pitch, and yaw angles and EMG signals are also shown in the figure.

Another design extends a 15 cm dipole antenna in order to achieve a complete battery-less operation. As the dipole

antenna harvests more energy than the MIFA, the system enables battery-less operation up to 50 cm using the dipole antenna (Figures S7 and S8 and Note S2, Supporting Information). The system is attached to an arbitrary paper-based object and utilized as a battery-less/wireless controller as shown in Figure S9 and Video S4 (Supporting Information), the system successfully controlled the vehicle with an entirely battery-less environment.

## 2. Conclusions

To overcome the limitation of current skin electronics with fixed designs, we propose a new in situ and in operando electronics design change methodology for thin-film electronics development. SOA enables device optimization and customization by synchronizing the design and fabrication for concurrent system modification and upgrading upon need for

new functionality and user differences. A device using SOA can actively accommodate various user specifications, such as skin condition tracking, human physiological measurements, and VR applications, and can be extended to enable wireless/battery-less operation. Furthermore, SOA can simultaneously optimize the impedance of an unknown circuit, making intensive simulations dispensable. The proposed approach opens new possibilities for the efficient development of customizable skin-like electronics.

### 3. Experimental Section

**Synthesis of Silver Nanoparticle Ink:** 0.25 mol L<sup>-1</sup> of silver nitrate (99% Aldrich) was used as a precursor and dissolved with 0.02 mol L<sup>-1</sup> of polyvinylpyrrolidone (PVP, Mw = 10 000, Aldrich) in ethylene glycol (EG, 99.9%, Aldrich). The solution was stirred in a 150 °C reaction state until the synthesis was completed. The synthesized particles were then separated for 30 min by 7000 rpm centrifugation, and washed with ethanol. The particles obtained were redispersed in ethanol at a 20 wt% concentration.

**Selective Laser Process of Metal Nanoparticles:** The optical system consisted of 355 nm pulsed laser (Nanio Air 355-3-V, InnoLas Photonics), 532 nm continuous laser (Sprout-G-5W, Lighthouse Photonics), and galvano-mirror (hurrySCAN II, Scanlab). Half-wave plate (HWP) and polarizing beam splitter (PBS) were installed for delicate laser power management (Figure S11, Supporting Information).

**Fabrication Conditions for SOA:** CPI substrate was prepared in a condition of 1400 rpm and 1 min of spin-coating, followed by 150 °C/30 min and 300 °C/30 min of annealing. Synthesized AgNP ink was spin-coated on a CPI substrate with a condition of 200 rpm and 1 min, which allowed fine deposition and evaporation of solvents. The particle was sintered at a scan speed of 400 mm s<sup>-1</sup> at a laser power of 80 mW for the writing process, and the resultant linewidth of the sintered Ag electrode was 20 μm with fine adhesion to the substrate (Figure S15, Supporting Information). Electrode was erased in a condition of 26 mW power at a scan speed of 50 mm s<sup>-1</sup> with a frequency of 30 kHz, and this condition ablated the electrode with 10 μm of linewidth. Chips were mounted above the stencil patterned conductive pastes (Figures S12 and S13 and Note S3, Supporting Information).

**Experimental Specifics of Rapid VIA Fabrication:** At an identical experimental setup as the erasing process, the scanning speed was reduced to 20 mm s<sup>-1</sup> to provide a higher energy density that was sufficient to remove the CPI substrate and eventually create a through hole. The depth of the VIA was easily manipulated through adjusting the laser power.

**Embedded System Programming:** The programming of the BLE-mixed MCU (CC2650RSM, Texas Instruments) was based on the manufacturer's official Integrated Development Environment (Code Composer Studio version 9.3.0, Texas Instrument) and Software Development Kit (BLE SDK 2.2.1, Texas Instrument). Calibration and operation of each sensor was conducted based on the manufacturer's datasheets (Table S1, Supporting Information) and logged by the computer through wireless communication at 50 Hz in real-time.

**Real-Time Virtual Reality Application:** The synchronization program was developed on the 3D VR/AR game modeling platform (Unity, unity.com). The 3D posture of the virtual arm and the grasping motion of the hand were determined based on the Euler angles measured by IMU sensor, and the magnitude of EMG signals, respectively.

**FEM Simulation of Antenna:** The parametric analysis of the antenna was performed through FEM simulation (CST Studio Suite, Dassault Systems). Under 50 Ω discrete port, various characteristics such as antenna performance, directivity, and impedance were achieved.

**S-Parameter Measurement:** S11 parameters of the system were measured through vector network analyzer (e5071b, Agilent Technologies). Device demonstration on skin: The person displayed in Figure 1,3,4 (K.K.K.) acknowledges and agrees with the use of his

image in this article. Informed signed consent was obtained from the volunteers prior to participation in this study.

### Supporting Information

Supporting Information is available from the Wiley Online Library or from the author.

### Acknowledgements

This work was supported by the National Research Foundation of Korea (NRF) Grants (NRF-2016R1A5A1938472 and 2021R1A2B5B03001691). All experiments in this research associated with the human experiment were consulted and approved by the institutional review board (IRB) of Seoul National University (Approval number: 2009/003-023).

### Conflict of Interest

The authors declare no conflict of interest.

### Author Contributions

K.K.K. and J.C. contributed equally to this work. K.K.K., J.C., and S.H.K. conceived and initiated the study. K.K.K. and J.C. designed and performed experiments. S.H.K. motivated and supervised the research program. J.H.K. and S.N. assisted in the development of wireless transmission system. All authors discussed the results and worked on the manuscript.

### Data Availability Statement

Research data are not shared.

### Keywords

customizable sensors, in operando optimization, skin-like electronics, thin-film electronics

Received: July 1, 2021  
Revised: August 1, 2021  
Published online:

- [1] Z. Zhou, K. Chen, X. Li, S. Zhang, Y. Wu, Y. Zhou, K. Meng, C. Sun, Q. He, W. Fan, E. Fan, Z. Lin, X. Tan, W. Deng, J. Yang, J. Chen, *Nat. Electron.* **2020**, *3*, 571.
- [2] I. You, D. G. Mackanic, N. Matsuhisa, J. Kang, J. Kwon, L. Beker, J. Mun, W. Suh, T. Y. Kim, J. B.-H. Tok, Z. Bao, U. Jeong, *Science* **2020**, *370*, 961.
- [3] Y. Ling, T. An, L. W. Yap, B. Zhu, S. Gong, W. Cheng, *Adv. Mater.* **2020**, *32*, 1904664.
- [4] M. Kaltenbrunner, M. S. White, E. D. Głowacki, T. Sekitani, T. Someya, N. S. Sariciftci, S. Bauer, *Nat. Commun.* **2012**, *3*, 770.
- [5] M. Kaltenbrunner, T. Sekitani, J. Reeder, T. Yokota, K. Kuribara, T. Tokuhara, M. Drack, R. Schwödiauer, I. Graz, S. Bauer-Gogonea, S. Bauer, T. Someya, *Nature* **2013**, *499*, 458.
- [6] H. Lin, J. Tan, J. Zhu, S. Lin, Y. Zhao, W. Yu, H. Hojajii, B.o Wang, S. Yang, X. Cheng, Z. Wang, E. Tang, C. Yeung, S. Emaminejad, *Nat. Commun.* **2020**, *11*, 4405.

- [7] Z. Huang, Y. Hao, Y. Li, H. Hu, C. Wang, A. Nomoto, T. Pan, Y. Gu, Y. Chen, T. Zhang, W. Li, Y. Lei, N. Kim, C. Wang, L. Zhang, J. W. Ward, A. Maralani, X. Li, M. F. Durstock, A. Pisano, Y. Lin, S. Xu, *Nat. Electron.* **2018**, *1*, 473.
- [8] K.-I.n Jang, K. Li, H.a U.k Chung, S. Xu, H. N.a Jung, Y. Yang, J. W. Kwak, H. H. Jung, J. Song, C.e Yang, A.o Wang, Z. Liu, J. Y. Lee, B. H. Kim, J.-H. Kim, J. Lee, Y. Yu, B. J. Kim, H. Jang, K.i J. Yu, J. Kim, J. W. Lee, J.-W. Jeong, Y. M. Song, Y. Huang, Y. Zhang, J. A. Rogers, *Nat. Commun.* **2017**, *8*, 15894.
- [9] K. Lee, X. Ni, J. Y. Lee, H. Arafa, D. J. Pe, S. Xu, R. Avila, M. Irie, J. H. Lee, R. L. Easterlin, D. H. Kim, H.a U.k Chung, O. O. Olabisi, S. Getaneh, E. Chung, M. Hill, J. Bell, H. Jang, C. Liu, J. B. Park, J. Kim, S. B. Kim, S. Mehta, M. Pharr, A. Tzavelis, J. T. Reeder, I. Huang, Y. Deng, Z. Xie, C. R. Davies, Y. Huang, J. A. Rogers, *Nat. Biomed. Eng.* **2020**, *4*, 148.
- [10] H.a U.k Chung, A. Y. Rwei, A. Hourlier-Fargette, S. Xu, K. Lee, E. C. Dunne, Z. Xie, C. Liu, A. Carlini, D. H. Kim, D. Ryu, E. Kulikova, J. Cao, I. C. Odland, K. B. Fields, B. Hopkins, A. Banks, C. Ogle, D. Grande, J. B. Park, J. Kim, M. Irie, H. Jang, J. Lee, Y. Park, J. Kim, H. H. Jo, H. Hahm, R. Avila, Y. Xu, M. Namkoong, J. W. Kwak, E. Suen, M. A. Paulus, R. J. Kim, B. V. Parsons, K. A. Human, S. S. Kim, M. Patel, W. Reuther, H. S. Kim, S. H. Lee, J. D. Leedle, Y. Yun, S. Rigali, T. Son, I. Jung, H. Arafa, V. R. Soundararajan, A. Ollech, A. Shukla, A. Bradley, M. Schau, C. M. Rand, L. E. Marsillio, Z. L. Harris, Y. Huang, A. Hamvas, A. S. Paller, D. E. Weese-Mayer, J. Y. Lee, J. A. Rogers, *Nat. Med.* **2020**, *26*, 418.
- [11] A. Miyamoto, S. Lee, N. F. Cooray, S. Lee, M. Mori, N. Matsuhisa, H. Jin, L. Yoda, T. Yokota, A. Itoh, M. Sekino, H. Kawasaki, T. Ebihara, M. Amagai, T. Someya, *Nat. Nanotechnol.* **2017**, *12*, 907.
- [12] Y.u R.a Jeong, J. Kim, Z. Xie, Y. Xue, S. M. Won, G. Lee, S. W. Jin, S. Y. Hong, X. Feng, Y. Huang, J. A. Rogers, J. S. Ha, *NPG Asia Mater.* **2017**, *9*, e443.
- [13] S. Choi, S. I. Han, D. Jung, H. J. Hwang, C. Lim, S. Bae, O. K. Park, C. M. Tschabrunn, M. Lee, S. Y. Bae, J. W. Yu, J. H. Ryu, S.-W. Lee, K. Park, P. M. Kang, W. B. Lee, R. Nezafat, T. Hyeon, D.-H. Kim, *Nat. Nanotechnol.* **2018**, *13*, 1048.
- [14] X. Yu, Z. Xie, Y. Yu, J. Lee, A. Vazquez-Guardado, H. Luan, J. Ruban, X. Ning, A. Akhtar, D. Li, B. Ji, Y. Liu, R. Sun, J. Cao, Q. Huo, Y. Zhong, C. Lee, S. Kim, P. Gutruf, C. Zhang, Y. Xue, Q. Guo, A. Chempakasseril, P. Tian, W. Lu, J. Jeong, Y. Yu, J. Cornman, C. Tan, B. Kim, K. Lee, X. Feng, Y. Huang, J. A. Rogers, *Nature* **2019**, *575*, 473.
- [15] S. Niu, N. Matsuhisa, L. Beker, J. Li, S. Wang, J. Wang, Y. Jiang, X. Yan, Y. Yun, W. Burnett, A. S. Y. Poon, J. B.-H. Tok, X. Chen, Z. Bao, *Nat. Electron.* **2019**, *2*, 361.
- [16] S. Han, J. Kim, S. M. Won, Y. Ma, D. Kang, Z. Xie, K.-T. Lee, H.a U.k Chung, A. Banks, S. Min, S. Y. Heo, C. R. Davies, J. W. Lee, C.-H. Lee, B. H. Kim, K. Li, Y. Zhou, C. Wei, X. Feng, Y. Huang, J. A. Rogers, *Sci. Transl. Med.* **2018**, *10*, eaan4950.
- [17] G. Casula, G. Montisci, *Electronics* **2019**, *8*, 244.
- [18] A. Kumar, R. K. Badhai, P. Suraj, *J. Comput. Electron.* **2018**, *17*, 1741.
- [19] X. Huang, Y. Liu, H. Cheng, W.-J. Shin, J. A. Fan, Z. Liu, C.-J. Lu, G.-W. Kong, K. Chen, D. Patnaik, S.-H. Lee, S. Hage-Ali, Y. Huang, J. A. Rogers, *Adv. Funct. Mater.* **2014**, *24*, 3846.
- [20] S. Risco, J. Anguera, A. Andújar, C. Picher, J. Pajares, *Microwave Opt. Technol. Lett.* **2012**, *54*, 454.
- [21] J. Kim, A. Banks, Z. Xie, S. Y. Heo, P. Gutruf, J. W. Lee, S. Xu, K.-I.n Jang, F. Liu, G. Brown, J. Choi, J. H. Kim, X. Feng, Y. Huang, U. Paik, J. A. Rogers, *Adv. Funct. Mater.* **2015**, *25*, 4761.
- [22] J. Byun, Y. Lee, J. Yoon, B. Lee, E. Oh, S. Chung, T. Lee, K.-J. Cho, J. Kim, Y. Hong, *Sci. Rob.* **2018**, *3*, eaas9020.
- [23] Y.-T. Kwon, Y.-S. Kim, S. Kwon, M. Mahmood, H.-R. Lim, S.-i-W. Park, S.-O. Kang, J. J. Choi, R. Herbert, Y. C. Jang, Y.-H.o Choa, W.-H. Yeo, *Nat. Commun.* **2020**, *11*, 3450.
- [24] E. Balliu, H. Andersson, M. Engholm, T. Öhlund, H.-E. Nilsson, H. Olin, *Sci. Rep.* **2018**, *8*, 10408.
- [25] P. Won, J. J. Park, T. Lee, I. Ha, S. Han, M. Choi, J. Lee, S. Hong, K.-J. Cho, S. H. Ko, *Nano Lett.* **2019**, *19*, 6087.
- [26] S. Yang, Y.-C. Chen, L. Nicolini, P. Pasupathy, J. Sacks, B. Su, R. Yang, D. Sanchez, Y.-F. Chang, P. Wang, D. Schnyer, D. Neikirk, N. Lu, *Adv. Mater.* **2015**, *27*, 6423.
- [27] Z. Xie, R. Avila, Y. Huang, J. A. Rogers, *Adv. Mater.* **2020**, *32*, 1902767.
- [28] M. Lee, S. Lim, *Sensors* **2018**, *18*, 3176.
- [29] M.d A. Islam, A. Kiourti, J. L. Volakis, *IEEE Sens. J.* **2015**, *16*, 265.
- [30] F. Merli, B. Fuchs, J. R. Mosig, A. K. Skrivervik, *IEEE Trans. Antennas Propag.* **2010**, *59*, 21.
- [31] K. K. Kim, I. Ha, P. Won, D.-G. Seo, K.-J. Cho, S. H. Ko, *Nat. Commun.* **2019**, *10*, 2582.
- [32] V.u B. Nam, J. Shin, Y. Yoon, T. T. Giang, J. Kwon, Y. D. Suh, J. Yeo, S. Hong, S. H. Ko, D. Lee, *Adv. Funct. Mater.* **2019**, *29*, 1806895.